

# Reversed propagation dynamics of Laguerre-Gaussian beams in left-handed materials

Hailu Luo<sup>1,2,\*</sup>, Zhongzhou Ren<sup>1</sup>, Weixing Shu<sup>2</sup>, and Shuangchun Wen<sup>2</sup>

<sup>1</sup> *Department of Physics, Nanjing University, Nanjing 210008, China*

<sup>2</sup> *School of Computer and Communication, Hunan University, Changsha 410082, China*

(Dated: October 23, 2018)

On the basis of angular spectrum representation, the reversed propagation dynamics of Laguerre-Gaussian beam in left-handed materials (LHMs) is presented. We show that negative phase velocity gives rise to a reversed screw of wave-front, and ultimately leads to a reversed rotation of optical vortex. Furthermore, negative Gouy-phase shift causes an inverse spiral of Poynting vector. It is found that the Laguerre-Gaussian beam in LHMs will present the same propagation characteristics as the counterpart with opposite topological charges in regular right-handed materials (RHMs). The momentum conservation theorem insures that the tangential component of the wave momentum at the RHM-LHM boundary is conserved. It is shown that although the linear momentum reverses its direction, the angular momentum remains unchanged.

PACS numbers: 42.25.-p; 42.79.-e; 41.20.Jb; 78.20.Ci

Keywords: Left-handed material; Laguerre-Gaussian beam; Poynting vector; Angular momentum

## I. INTRODUCTION

Almost 40 years ago, Russian scientist Victor Veselago proposed that a material with electric permittivity  $\varepsilon < 0$  and magnetic permeability  $\mu < 0$ , would reverse all known optical properties [1]. He termed these media as left-handed materials (LHMs) since the wave vector  $\mathbf{k}$ , forms a left-handed triplet with the vectors  $\mathbf{E}$  and  $\mathbf{H}$ . That is, phase velocity and the Poynting vector are antiparallel, which consequently results in counter-intuitive phenomena such as reversals of the conventional Doppler shift and Cherenkov radiation as well as reversed refraction. Veselago pointed out that electromagnetic waves incident on a planar interface between a regular right-handed material (RHM) and a LHM will undergo negative refraction. Hence a LHM planar slab can act as a lens and focus waves from a point source. Recently, Pendry extended Veselago's analysis and further predicted that a LHM slab can amplify evanescent waves and thus behaves like a perfect lens [2]. Pendry proposed that the amplitudes of evanescent waves from a near-field object could be restored at its image. Therefore, the spatial resolution of the superlens can overcome the diffraction limit of conventional imaging systems and reach the sub-wave length scale. The physical realization of such a LHM was demonstrated only recently for a novel class of engineered composite materials [3, 4, 5, 6].

After the first experimental observation of negative refraction, intriguing and counterintuitive phenomenon in LHMs, such as amplification of evanescent waves [2, 7], unusual photon tunneling [8, 9], and negative Goos-Hänchen shift [10, 11] have attracted much attention. Here we want to explore the reversed propagation dynamics of Laguerre-Gaussian beams in LHMs. The propagation of Laguerre-Gaussian beam has been investigated in conventional RHMs [12, 13, 14, 15]. Such beams have a

phase dislocation on the beam axis that in related literature is sometimes referred to as an optical vortex [14]. For a general Laguerre-Gaussian beam the Poynting vector has an azimuthal component. This means that there is an energy flow along the circumference of the beam as it propagates, giving rise to an orbital angular momentum [16]. It is found that the spiral of the Poynting vector of a Laguerre-Gaussian beam is proportional to the Gouy-phase shift [17, 18]. It is known that an electromagnetic beam propagating through a focus experiences an additional  $\pi$  phase shift with respect to a plane wave. This phase anomaly was discovered by Gouy in 1890 and has since been referred to as the Gouy-phase shift [19]. Because of the negative index, however, we can expect an reversed Gouy-phase shift in LHMs [20]. Hence it will be interesting for us to describe in detail how the Poynting vector evolves as it propagates and how the reversed Gouy-phase shift affects its spiral in LHMs.

In this work, we will reveal reversed propagation dynamics of Laguerre-Gaussian beam in LHMs, such as inverse screw of wave-front, inverse spiral of Poynting vector, and inverse rotation of vortex field. First, starting from the representation of plane-wave angular spectrum, we obtain the analytical description for a Laguerre-Gaussian beam propagating in LHMs. Our formalism permits us to introduce the reversed Gouy-phase shift to describe the wave propagation. Next, we will recover how the wave-front and Poynting vector evolves, and how the reversed Gouy-phase shift affects their propagation behavior. Then, we attempt to investigate how the negative index influences the linear momentum and angular momentum of Laguerre-Gaussian beams. Finally, we will explore how the negative index gives rise to the reversed rotation of the vortex field. For a comparison, the corresponding propagation characteristics in RHMs will also be discussed.

---

\*Electronic address: hailuluo@gmail.com

## II. THE PARAXIAL PROPAGATION OF A LAGUERRE-GAUSSIAN BEAM

To investigate the propagation dynamics of a Laguerre-Gaussian beam in LHMs, we use the Maxwell's equations to determine the field distribution both inside and outside the LHM. We consider a monochromatic electromagnetic field  $\mathbf{E}(\mathbf{r}, t) = \text{Re}[\mathbf{E}(\mathbf{r}) \exp(-i\omega t)]$  and  $\mathbf{B}(\mathbf{r}, t) = \text{Re}[\mathbf{B}(\mathbf{r}) \exp(-i\omega t)]$  of angular frequency  $\omega$  propagating from the RHM to the LHM. The field can be described by Maxwell's equations

$$\begin{aligned} \nabla \times \mathbf{E} &= -\frac{\partial \mathbf{B}}{\partial t}, & \mathbf{B} &= \mu_0 \boldsymbol{\mu} \cdot \mathbf{H}, \\ \nabla \times \mathbf{H} &= \frac{\partial \mathbf{D}}{\partial t}, & \mathbf{D} &= \varepsilon_0 \boldsymbol{\varepsilon} \cdot \mathbf{E}. \end{aligned} \quad (1)$$

From the Maxwell's equations, we can easily find that the wave propagation is only permitted in the medium with  $\varepsilon, \mu > 0$  or  $\varepsilon, \mu < 0$ . In the former case,  $\mathbf{E}$ ,  $\mathbf{H}$  and  $\mathbf{k}$  form a right-handed triplet, while in the latter case,  $\mathbf{E}$ ,  $\mathbf{H}$  and  $\mathbf{k}$  form a left-handed triplet.

We introduce the Lorentz-gauge vector potential to describe the propagation characteristics of Laguerre-Gaussian in RHMs and LHMs. The vector potential of the beam propagating in the  $+z$  direction can be written in the form

$$\mathbf{A} = A_0(\alpha \mathbf{e}_x + \beta \mathbf{e}_y) u_{p,l}(\mathbf{r}) \exp(ikz - i\omega t), \quad (2)$$

where  $A_0$  is a complex amplitude,  $\mathbf{e}_x$  and  $\mathbf{e}_y$  are unit vectors,  $k = n_{R,L}\omega/c$ ,  $c$  is the speed of light in vacuum,  $n_R = \sqrt{\varepsilon_R \mu_R}$  and  $n_L = -\sqrt{\varepsilon_L \mu_L}$  are the refractive index of RHM and LHM, respectively [1]. The coefficients  $\alpha$  and  $\beta$  satisfying  $\sigma = i(\alpha\beta^* - \alpha^*\beta)$ , are the polarization operators with  $\sigma = \pm 1$  for left-handed and right-handed circularly polarized light.

When the field distribution is specified at a boundary surface or a transverse plane, one can obtain a unique solution of the electric field of the wave propagating in the  $+z$  direction. Here, we assume that the transverse electric field at the  $z = 0$  plane is given by a Laguerre-Gaussian function as follows:

$$u(r, \varphi, 0) = \frac{C_{pl}}{w_0} \left[ \frac{\sqrt{2}r}{w_0^2} \right]^{|l|} L_p^{|l|} \left[ \frac{2r^2}{w_0^2} \right] \exp \left[ \frac{r^2}{w_0^2} - il\varphi \right]. \quad (3)$$

A Laguerre-Gaussian beam has two mode indices to fully describe the mode:  $l$  and  $p$ . A given mode will have  $l$  complete cycles of phase  $2\pi$  upon going around the mode circumference, so that  $l$  is known as the azimuthal index. The index  $p$  gives the number  $p + 1$  of radial nodes. Laguerre-Gaussian light beams are well known to possess orbital angular momentum due to an  $\exp[il\varphi]$  phase term, where  $\varphi$  is the azimuthal phase. This orbital angular momentum  $l\hbar$  is distinct from the spin angular momentum due to the polarization state of the light [16].

From the point of view of Fourier optics, we know that if the Fourier component at the  $z = 0$  plane represents the angular spectrum that the transverse component of

the wave propagating in the half space  $z > 0$  should have. Then, the field in the region  $z > 0$  can be expressed by an integral of the plane wave components associated with the angular spectrum given at the  $z > 0$  plane [21]. The angular spectrum is related to the boundary distribution of the field by means of the relation

$$\tilde{u}(k) = \int_0^\infty dr r J_l(kr) u(r, \varphi, 0), \quad (4)$$

where  $J_l$  is the first kind of Bessel function with order  $l$ . The two-dimensional Fourier transformations of Eq.(4) can be easily obtained from an integration table [22]. In fact, after the field on the plane  $z = 0$  is known, Eq. (3) together with Eq. (4) provides the expression of the field in the space  $z > 0$ , which yields

$$u(r, \varphi, z) = \int_0^\infty dk k \exp \left( -\frac{ik^2 z}{2n_{R,L}k_0} \right) J_l(kr) \tilde{u}(k). \quad (5)$$

which is a standard two-dimensional Fourier transform [21]. The field  $u(\mathbf{r}, z)$  is the slowly varying envelope amplitude which satisfies the paraxial wave equation

$$\left[ i \frac{\partial}{\partial z} + \frac{1}{2n_{R,L}k_0} \nabla_\perp^2 \right] u(\mathbf{r}, z) = 0, \quad (6)$$

where  $\nabla_\perp = \partial_x \mathbf{e}_x + \partial_y \mathbf{e}_y$ . From Eq. (6) we can find that the field of paraxial beam in LHMs can be written in the similar way to that in RHMs, while the sign of the refractive index is negative.

The gauge condition on the vector and scalar potentials takes the form  $\phi = (i/k)\nabla \cdot \mathbf{A}$ . The electric and magnetic fields are obtained from the potentials as

$$\begin{aligned} \mathbf{E}(\mathbf{r}, t) &= -\frac{\partial \mathbf{A}}{\partial t} - \nabla \phi = A_0 \left[ i\omega(\alpha \mathbf{e}_x + \beta \mathbf{e}_y) u \right. \\ &\quad \left. - \left( \alpha \frac{\partial u}{\partial x} + \beta \frac{\partial u}{\partial y} \right) \mathbf{e}_z \right] \exp(ikz - i\omega t), \end{aligned} \quad (7)$$

$$\begin{aligned} \mathbf{B}(\mathbf{r}, t) &= \nabla \times \mathbf{A} = A_0 \left[ -ik(\beta \mathbf{e}_x - \alpha \mathbf{e}_y) u \right. \\ &\quad \left. + \left( \beta \frac{\partial u}{\partial x} - \alpha \frac{\partial u}{\partial y} \right) \mathbf{e}_z \right] \exp(ikz - i\omega t). \end{aligned} \quad (8)$$

These field expressions neglect terms in each component that are smaller than those retained in accordance with the paraxial approximation [23]. The  $z$  components are smaller than the  $x$  and  $y$  components by a factor of order  $1/kw_0$ . It is readily verified that the fields satisfy Maxwell's equations. Note that the Cartesian derivatives can be converted to polar  $r$  and  $\varphi$  derivatives in the usual way.

To be uniform throughout the following analysis, we introduce different coordinate transformations  $z_i^*$  ( $i = 1, 2$ ) in the RHM and the LHM, respectively. First we want to explore the field in the RHM. Without any loss of generality, we assume that the input waist locates at the

object plane  $z = -a$  and  $z_1^* = z + a$ . The field in the RHM can be written as

$$u_{pl}^R = \frac{C_{pl}}{w(z_1^*)} \left[ \frac{\sqrt{2}r}{w^2(z_1^*)} \right]^{|l|} L_p^{|l|} \left[ \frac{\sqrt{2}r}{w^2(z_1^*)} \right] \exp \left[ \frac{-r^2}{w^2(z_1^*)} \right] \times \exp \left[ in_R k_0 z_1^* + \frac{-in_R k_0 r^2 z_1^*}{R(z_1^*)} \right] \exp[-il\varphi] \times \exp[-i(2p + |l| + 1) \arctan(z_1^*/z_R)], \quad (9)$$

$$w(z_1^*) = w_0 \sqrt{1 + (z_1^*/z_R)^2}, \quad R(z_1^*) = z_1^* + \frac{z_R^2}{z_1^*}. \quad (10)$$

Here  $C_{pl}$  is the normalization constant,  $L_p^l[2r^2/w_1^2(z_1^*)]$  is a generalized Laguerre polynomial,  $z_R = n_R k_0 w_0^2/2$  is the Rayleigh length,  $w(z_1^*)$  is the beam size and  $R(z_1^*)$  the radius of curvature of the wave front. The last term in Eq. (9) denotes the Gouy phase which is given by  $\Phi_1 = -(2p + |l| + 1) \arctan(z_1^*/z_R)$ .

We are now in a position to calculate the field in LHM. In fact, the field in the RHM-LHM boundary can be easily obtained from Eq. (9) by choosing  $z = 0$ . The plane-wave spectrum of the Laguerre-Gaussian beam can be obtained by performing the two-dimensional Fourier transform in Eq. (4). After the plane-wave spectrum on the plane  $z = 0$  is known, Eq. (5) provides the expression of the field in the space  $z > 0$ . For simplicity, we assume that the wave propagates through the boundary without reflection, the field in the LHM can be written as

$$u_{pl}^L = \frac{C_{pl}}{w(z_2^*)} \left[ \frac{\sqrt{2}r}{w^2(z_2^*)} \right]^{|l|} L_p^{|l|} \left[ \frac{\sqrt{2}r}{w^2(z_2^*)} \right] \exp \left[ \frac{-r^2}{w^2(z_2^*)} \right] \times \exp \left[ in_L k_0 z_2^* + \frac{-in_L k_0 r^2}{R(z_2^*)} \right] \exp[-il\varphi] \times \exp[-i(2p + |l| + 1) \arctan(z_2^*/z_L)], \quad (11)$$

$$w(z_2^*) = w_0 \sqrt{1 + (z_2^*/z_L)^2}, \quad R(z_2^*) = z_2^* + \frac{z_L^2}{z_2^*}. \quad (12)$$

Here  $z_2^* = z - (1 - n_L/n_R)a$  and  $z_L = n_L k_0 w_0^2/2$  is the Rayleigh length in LHM. The beam size  $w(z_2^*)$  and the radius of curvature  $R(z_2^*)$  are given by Eq. (12). The Gouy-phase shift in LHM is given by  $\Phi_G = -(2p + |l| + 1) \arctan(z_2^*/z_L)$ . Because of the negative index, the reversed Gouy-phase shift should be introduced. A more intuitive interpretation of the reversed Gouy phase can be given in terms of a geometrical quantum effect [24] or the uncertainty principle [25]. As can be seen in the following section, the inverse Gouy-phase shift will give rise to an inverse spiral of Poynting vector.

For a Laguerre-Gaussian beam with  $l \neq 0$ , the on-axis phase form  $\exp[il\varphi]$  results in that the surfaces of wavefront have helical form. Specifically,  $l$  refers to the number of complete cycles of phase  $2\pi$  upon going around the beam circumference. Now let us to study the screw of the wave front. Here the sense of the positive angles

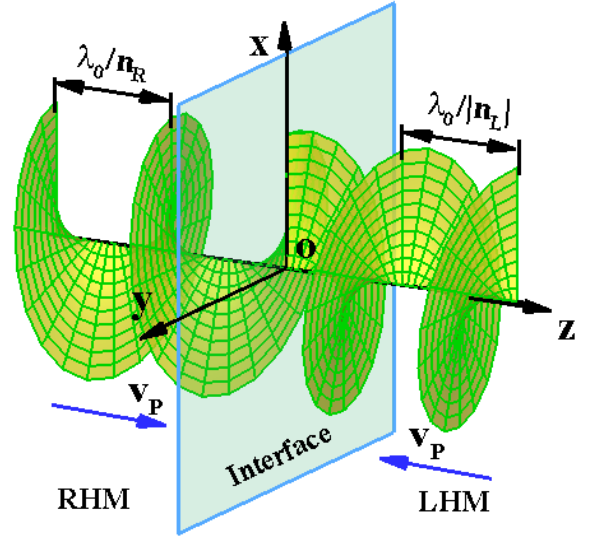


FIG. 1: (Color online) The helical wave front for Laguerre-Gaussian beam with  $l = 1$  result from an azimuthal phase structure of  $\exp[-i\varphi]$ . In the LHM, the phase velocity  $\mathbf{v}_p$  reverses its direction. The wave-fronts exhibit anti-clockwise screw in the RHM, while present clockwise screw in the LHM.

is chosen as anticlockwise, while negative angles are considered in the clockwise direction. In the regular RHM, the constant wavefront satisfies

$$n_R k_0 z_1^* + \frac{-in_R k_0 r^2}{R(z_1^*)} - l\varphi + \Phi_G = const. \quad (13)$$

The schematic view of the wave front is a three-dimensional screw surface of  $(r \cos \varphi, r \sin \varphi, z)$ . The plotting range of  $r$  is from 0 to  $5w_0$  with the interval of  $\Delta r = 0.5w_0$  and that of  $n_R k_0 z$  is from  $-4\pi$  to 0 with the interval of  $n_R k_0 \Delta z = 0.1\pi$ . The wavefront structure exhibits a anticlockwise-screw type with a pitch of  $\lambda_0/n_R$  along the  $+z$  axis.

Next we explore the screwing fashion of wave front in the LHM. The constant wavefront satisfies

$$n_L k_0 z_2^* + \frac{-in_L k_0 r^2}{R(z_2^*)} - l\varphi + \Phi_G = const. \quad (14)$$

The plotting range of  $r$  is from 0 to  $5w_0$  with the interval of  $\Delta r = 0.5w_0$  and that of  $n_L k_0 z$  is from 0 to  $-4\pi$  with the interval of  $n_L k_0 \Delta z = -0.1\pi$ . The wavefront structure is a clockwise-screw type with a pitch of  $\lambda_0/|n_L|$  along the  $+z$  axis. Figure 2 shows a typical form of a helical wavefront structure from the RHM to the LHM. At the RHM-LHM interface, the wave front will reverse its screwing fashion. It is intriguing to observe that the wave-front of Laguerre-Gaussian beam with  $l = 1$  in LHMs will exhibit the same skewing fashion as the counterpart with  $l = -1$  in RHMs. As can be seen in the following section, the inverse screw of wavefront will result in an inverse rotation of optical vortex.

### III. POYNTING VECTOR AND ANGULAR MOMENTUM

The propagation characteristics of electromagnetic fields are closely linked to their local energy flow, which is usually discussed by use of the Poynting vector. There has been considerable interest in orbital angular momentum of Laguerre-Gaussian beams [16] relating to Poynting vector in free space. The Poynting vector has a magnitude of energy per second per unit area and a direction which represents the energy flow at any point in the field. The time average Poynting vector,  $\mathbf{S}$  can be written as

$$\mathbf{S} = \frac{1}{2}\text{Re}[\mathbf{E} \times \mathbf{H}^*]. \quad (15)$$

The spiral of the Poynting vector in free space or regular RHMs has been discussed extensively [16, 17, 18, 26, 27, 28].

Now a question arise: what happens in LHMs with simultaneously negative permeability and permittivity? The potential interests encourage us to derive a general expression to describe the Poynting vector in RHMs and LHMs. Substituting the expression of Eqs. (7) and (8) into Eq. (15) we find

$$\begin{aligned} S_r &= \frac{1}{\mu\mu_0} \frac{\omega k r}{R} |u|^2, \\ S_\varphi &= \frac{1}{\mu\mu_0} \left[ \frac{\omega l}{r} |u|^2 - \frac{1}{2} \omega \sigma \frac{\partial |u|^2}{\partial r} \right], \\ S_z &= \frac{1}{\mu\mu_0} \omega k |u|^2. \end{aligned} \quad (16)$$

Here the component  $S_r$ , relates to the spread of the beam as it propagates. The azimuthal component  $S_\varphi$  describes the energy flow that circulates around the propagating axis. The presence of this flow is due to the existence of the longitudinal components  $E_z$  and  $H_z$  of the field. The first term of the azimuthal component depends on  $l$ , where  $l\hbar$  has been identified as the orbital angular momentum per photon [16]. Its second term relates to the contribution of polarization and intensity gradient. The contribution of circular polarization will lead to a spin angular momentum of the beam. The axial component  $S_z$  describes the energy flow that propagates along the  $+z$  axis.

Next, we attempt to explore the angular momentum in LHMs. Since the dispersion cannot be ignored in a causal system with a negative index of refraction. The momentum conservation theorem should be derived from the Maxwell equations and the Lorentz force and is given by [29]

$$\nabla \cdot \mathbf{T} + \frac{\partial \mathbf{G}}{\partial t} = -\mathbf{F}. \quad (17)$$

where  $\mathbf{G}$  is the momentum density vector and  $\mathbf{F}$  is the force density. The momentum flow  $\mathbf{T}$  also referred as the Maxwell stress tensor. It is well-known that a material contribution to the energy density accompanies the propagation of electromagnetic energy in dispersive materials.

Analogously, there exists a corresponding material contribution to the wave momentum. Thus the momentum conservation equation for the electromagnetic wave can be written in the form [30]

$$\begin{aligned} \mathbf{G} &= \frac{1}{2}\text{Re} \left[ \varepsilon\mu\mathbf{E} \times \mathbf{H}^* + \frac{\mathbf{k}}{2} \left( \frac{\partial\varepsilon}{\partial\omega} |\mathbf{E}|^2 + \frac{\partial\mu}{\partial\omega} |\mathbf{H}|^2 \right) \right], \\ \mathbf{T} &= \frac{1}{2}\text{Re}[(\mathbf{D} \cdot \mathbf{E}^* + \mathbf{B} \cdot \mathbf{H}^*)I - (\mathbf{D}\mathbf{E}^* + \mathbf{B}\mathbf{H}^*)], \\ \mathbf{F} &= \frac{1}{2}\text{Re}[\rho_e\mathbf{E}^* + \mathbf{J} \times \mathbf{B}^* + \rho_m\mathbf{H}^* + \mathbf{M} \times \mathbf{D}^*]. \end{aligned} \quad (18)$$

Here the momentum density  $\mathbf{G}$  contains the Minkowski momentum  $\mathbf{G}_M = \mathbf{D} \times \mathbf{B}$  plus material dispersion terms. The tensor  $I$  is  $3 \times 3$  identity matrix. The electric and magnetic polarization vectors are give by  $\mathbf{P}_e = \varepsilon_0(\varepsilon - 1)\mathbf{E}$  and  $\mathbf{P}_m = -\mu_0(\mu - 1)\mathbf{H}$ , respectively. Bound electric current  $\mathbf{J} = \partial\mathbf{P}_e/\partial t$  and bound electric charge  $\rho_e = \nabla \cdot \mathbf{P}_e$  have been accounted. Similarly, bound magnetic current  $\mathbf{M} = \partial\mathbf{P}_m/\partial t$  and bound magnetic charge  $\rho_m = \nabla \cdot \mathbf{P}_m$  should be introduced to describe the angular momentum flow in LHMs.

Now we want to enquire: how to determine directions of the momentum density and the momentum flow? It is well known that the time-domain energy density in a frequency nondispersive medium are defined as  $W = \frac{1}{2}[\mathbf{D} \cdot \mathbf{E} + \mathbf{E} \cdot \mathbf{H}]$ . Obviously, the energy density in LHMs would be negative if the permittivity and permeability were negative. Hence, the energy density in a frequency dispersive medium is defined as [31, 32]

$$W = \frac{1}{4} \left[ \frac{\partial(\varepsilon\omega)}{\partial\omega} |\mathbf{E}|^2 + \frac{\partial(\mu\omega)}{\partial\omega} |\mathbf{H}|^2 \right]. \quad (19)$$

In principle, the energy density can be decomposed into electric and magnetic parts. The positive electric and magnetic energy requires  $\partial(\varepsilon\omega)/\partial\omega > 0$  and  $\partial(\mu\omega)/\partial\omega > 0$ . Subsequent calculations of Eq. (18) show that both the momentum density  $\mathbf{G}$  and the momentum flow  $\mathbf{T}$  in LHMs are antiparallel to the power flow  $\mathbf{S} = \frac{1}{2}\text{Re}[\mathbf{E} \times \mathbf{H}^*]$ . Hence we conclude that the linear angular momentum flux will reverse its direction in LHMs. Note that Eqs. (18) and (19) are valid only for lossless media, and its application to lossy media produces unphysical phenomena such as a negative energy in LHMs. In a lossy and dispersive LHM, the momentum flow of a monochromatic wave is opposite to the power flow direction. However, the momentum density may be parallel or antiparallel to the power flow [33].

The cross product of this momentum density with the radius vector  $\mathbf{r}$  yields an angular momentum flow. The angular momentum flow in the  $z$  direction depends upon the component of  $\mathbf{G}_\varphi$ , such that

$$\mathbf{J}_z = \mathbf{r} \times \mathbf{T}_\varphi. \quad (20)$$

Conservation of momentum at a material boundary ensures that the tangential component of the wave momentum is conserved [30, 33]. Hence the angular momentum flow still remains unchanged in the LHM. We can predict

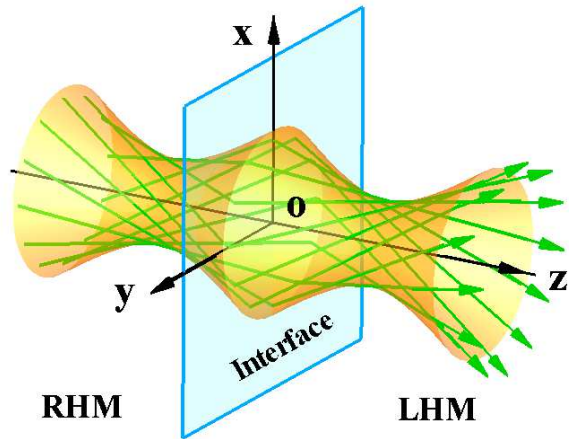


FIG. 2: (Color online) Ray optical model of Laguerre-Gaussian beam in the RHM and the LHM. The rays (green arrows) lies on a single-sheeted hyperboloid surface. Note that the arrows indicate the direction of the Poynting vectors. When Rays travel from a RHM to a LHM, the negative refraction results in the reversed screw. The rays exhibit anticlockwise screw in the RHM, while he rays present clockwise screw in the LHM.

theoretically that the orbital angular momentum for per phonon still remain  $\hbar l$ . In order to accurately describe the angular momentum flow, it is necessary to include material dispersion and losses. Thus a certain dispersion relation, such as Lorentz medium model, should be involved.

It has been shown that the trajectory at peak intensity becomes a straight line skewed with respect to the beam axis in RHMs [34]. To obtain a better physical picture of the straight trajectory in LHMs, the ray optical models of Laguerre-Gaussian beam are plotted in Fig. 2. Within a ray optical picture, the angular spectrum may be represented by skew rays in the optical beam. The screwing behavior of rays can be deduced from Eq. (16) in which we see that each ray having an azimuthal angle  $\theta = l/(n_{R,L}k_0r)$  and a polar angel  $\eta = r/R$  with respect to the beam axis. Hence all rays lies on a single-sheeted hyperboloid surface. Note that wave-vector and the Poynting vector are parallel in the RHM and antiparallel in the LHM. Energy conservation requires that the  $z$  component of Poynting vector must propagates away from the interface. Both wave-vector and energy flow incident on a planar interface between a RHM and a LHM will undergo negative refraction. Therefore all rays will reverse its screwing fashion in the LHM (see Fig. 2).

To explore the reversed propagation dynamics in the LHM, we need to move beyond ray tracing. The ray optical models neglect diffraction and thus could not be used to predict precisely the spiral of Poynting vector. To include diffraction, we had to use a more accurate description of the electromagnetic field. It is well known that the trajectory of the Poynting vector is described

by the spiral curve [16]. The relative value of the components determines the trajectory of the Poynting vector. The spiral angle of the Poynting vector is given by  $\theta = \theta_0 + \kappa z$ , where  $\kappa = \partial\theta/\partial z = S_\varphi/(rS_z)$  is the rate of rotation. The period of the trajectory along the  $z$  axis is  $2\pi/\kappa$ . For a general Laguerre-Gaussian beam, the rate of the azimuthal rotation is relate to the distance given by

$$\frac{\partial\theta}{\partial z} = \frac{l}{n_{R,L}k_0r^2} - \frac{\sigma|l|}{n_{R,L}k_0r^2} + \frac{2\sigma}{n_{R,L}k_0w^2(z)} + \frac{4\sigma}{n_{R,L}k_0w^2(z)} \frac{L_p^{|l+1|}[2r^2/w^2(z)]}{L_p^{|l|}[2r^2/w^2(z)]}. \quad (21)$$

Note that the first term is polarization independent. While the last three terms depends on the polarization. For modes with  $p = 0$ , the final term is always zero.

For a single-ringed Laguerre-Gaussian beam  $p = 0$  but  $l \neq 0$ , the scaled radius of the peak intensity is given by  $r_{max} = \sqrt{|l|/2w(z)}$ . We find that, for all values of  $l$  and  $\sigma$ , the rotation angle is given by

$$\theta_{max} = \frac{l}{|l|} \arctan \frac{z}{z_{R,L}}. \quad (22)$$

Figure 3 shows the vector fields illustrating the spiral angle of the Poynting vector. The Poynting vector exhibits anticlockwise spiral in the RHM as depicted in Fig. 3(a), while presents clockwise spiral in the LHM as plotted in Fig. 3(b). The theoretical analysis and numerical calculations presented here coincide with experimental observations [35]. For  $l \neq 0$ , Laguerre-Gaussian beam have annular intensity profiles and as  $r_{max}$  is typically much greater than optical wavelength  $\lambda$ , the skew angle is expected to be very small.

It can clearly be seen that the sense of spiral (clockwise or anticlockwise) depends on the signs of  $l$  and the Rayleigh length. However, the amount of rotation of the poynting vector is independent of the magnitude of  $l$ . It is interesting to note that the Laguerre-Gaussian beam in LHMs will present the same fashion of spiral as the counterpart with opposite topological charges in RHMs. This is consist with the ray optical model describing the spiral of the Poynting vector. Equation (22) implies that the absolute rotation for a single-ringed Laguerre-Gaussian beam at  $z = z_{R,L}$  is  $\pi/4$ , regardless of  $l$ . When the far-field pattern of Poynting vector is calculated it is found that the Poynting vector is spiraled by  $\pi/2$ .

When  $l = 0$  and  $p = 0$ , the Laguerre-Gaussian is identical to the fundamental Gaussian beam, the spiral of the Poynting vector arises from the effect of circular polarization [18]. The azimuthal rotations in the RHM and the LHM are relate to the distance can be obtained as  $\theta = \sigma \arctan(z/z_R)$  and  $\theta = \sigma \arctan(z/z_L)$ , respectively. It is intriguing to note that the right-handed circularly polarized beam in LHMs will present the same fashion of spiral as the left-handed circularly polarized beam in RHMs. Hence we can describe quantitatively the amount of spiral of the Poynting vector, from which we can determine whether a material is a LHM or a RHM.

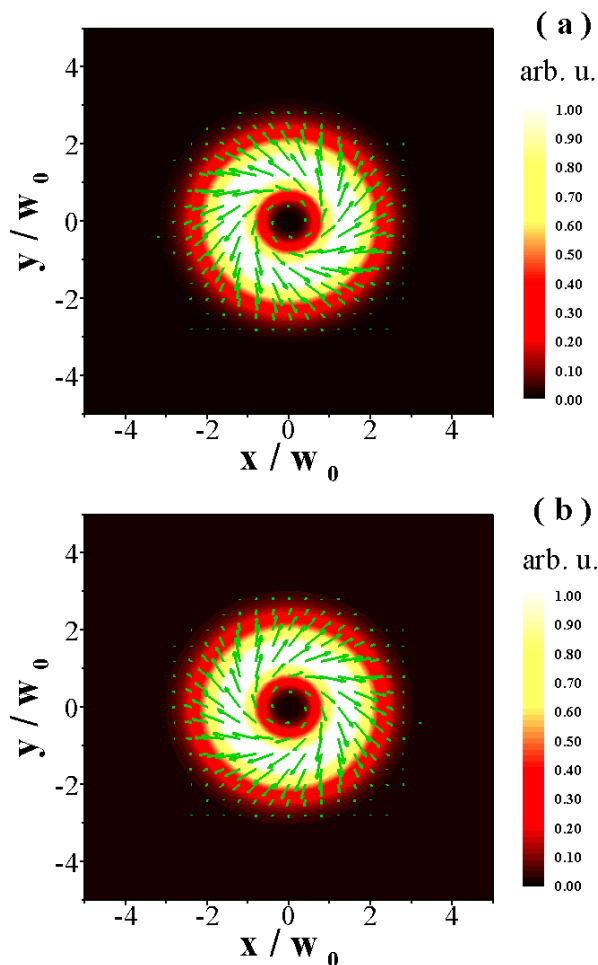


FIG. 3: (Color online) Numerically computed field intensity distribution and transversal components of Poynting vector (green arrows) for  $l = 3$  Laguerre-Gaussian beam. (a) The Poynting vector exhibits anticlockwise spiral in RHM  $z_1^* = n_R k_0 w_0^2 / 2$ . (b) The Poynting vector presents clockwise spiral in LHM  $z_2^* = |n_L| k_0 w_0^2 / 2$ . For the purpose of comparison, we have chosen  $n_L = -n_R$ .

Interfering the Laguerre-Gaussian beam with a fundamental Gaussian beam will transform the azimuthal phase variation of the pattern into an azimuthal intensity variation. Hence the helical phase ultimately results in a vortex field with  $|l|$  spiral arms [36, 37, 38]. The intriguing properties strongly motivate us to explore the vortex field propagation in LHMs. A simulation of the vortex field rotation produced by interfering a fundamental Gaussian beam and an Laguerre-Gaussian beam of azimuthal index  $l = 3$  is shown in Fig. 4. It can be seen that the vortex has three spiral arms, which is a result of the mismatch between the wave-fronts of the Laguerre-Gaussian beam and the Gaussian beam. The reversed screwing wave-fronts will directly cause an inverse rotation of the vortex filed in the LHM. The vortex will always has a spiral shape unless the wavefronts of the two beams have the same curvature. For example, the vortex field at a focusing waist will exhibit  $|l|$  intense

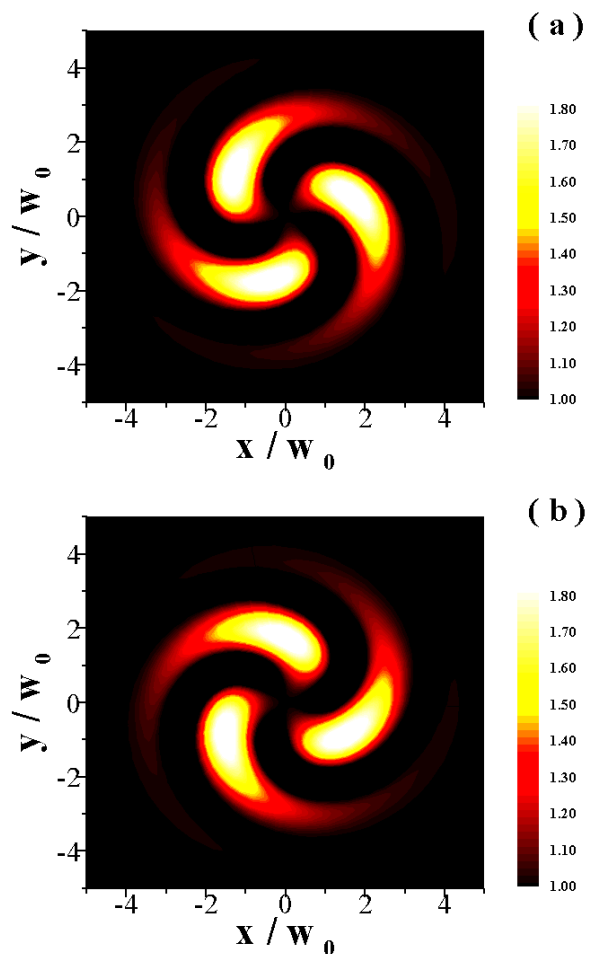


FIG. 4: (Color online) Interfering a Gaussian beam and a Laguerre-Gaussian beam of azimuthal index  $l = 3$  will produce the vortex field with three spiral arms. (a) The field distribution at plane of  $z_1^* = n_R k_0 w_0^2 / 2$ . (b) The field distribution at plane of  $z_2^* = |n_L| k_0 w_0^2 / 2$ . When the vortex field enters the LHM, the rotation changes its fashion.

spots. After the vortex propagating through the focusing waist, the spiral arms will change their shapes.

Now let us consider how to modulate the rotation of the vortex field. As we change the path length of the Gaussian beam, the spiral arms will rotate around the propagating axis. This is analogous to altering the phase different between the Laguerre-Gaussian beam and the Gaussian beam [38]. The spiral arms repeat every  $\lambda/|n_L|$  in the LHM, but only rotate fully after propagating  $|l|\lambda/|n_L|$ . A path length change in the Gaussian beam of  $3\lambda/|n_L|$  will cause the pattern to rotate through  $2\pi$  and  $-2\pi$  in RHM and LHM, respectively. The vortex presents an anticlockwise rotation in the RHM, while exhibits a clockwise rotation in the LHM. Once the vortex field enter the LHM, it will reverse its rotation fashion.

#### IV. CONCLUSIONS

In conclusion, we have investigated the reversed propagation dynamics of Laguerre-Gaussian beam in LHMs. We have introduced the concepts of negative Gouy-phase shift to describe the propagation of Laguerre-Gaussian beam in LHMs. The negative phase velocity and negative Gouy-phase shift caused inverse screw of wave-fronts, reversed spiral of Poynting vector, and inverse rotation of vortex field. At a RHM-LHM interface, direct calculation of Maxwell's equations dictates the wave-vector and energy flow undergoes negative refraction. Consequently, inside the LHMs, the screw of wave-fronts, the spiral of Poynting vector, and the rotation of vortex will reverse their direction. We have shown that the Poynting vector of Laguerre-Gaussian beam in LHMs will present the same fashion of spiral as the counterpart with opposite topological charges in RHMs. Conservation of momentum at the boundary ensure that the tangential compo-

nent of the wave momentum is conserved. We have found that although the linear momentum reverses its direction, the angular momentum still remains unchanged. Since the photons in Laguerre-Gaussian beam possess angular momentum, the reversed propagation dynamics may offer new fundamental insights into the nature of LHMs.

#### Acknowledgments

The authors are sincerely grateful to Professors Wei Hu and Zhenlin Wang for many fruitful discussions. This work was supported by projects of the National Natural Science Foundation of China (Grants Nos. 10535010, 10576012, 10674045, 10775068, and 60538010), the 973 National Major State Basic Research and Development of China (Grant No. G2000077400), and Major State Basic Research Developing Program (Grant No. 2007CB815000).

- 
- [1] V. G. Veselago, *Sov. Phys. Usp.* **10**, 509 (1968).
  - [2] J. B. Pendry, *Phys. Rev. Lett.* **85**, 3966 (2000).
  - [3] D. R. Smith, W. J. Padilla, D. C. Vier, S. C. Nemat-Nasser, S. Schultz, *Phys. Rev. Lett.* **84**, 4184 (2000).
  - [4] R. A. Shelby, D. R. Smith, S. Schultz, *Science* **292**, 77 (2001).
  - [5] C. G. Parazzoli, R. B. Greigor, K. Li, B. E. C. Koltenbah, M. Tanielian, *Phys. Rev. Lett.* **90**, 107401 (2003).
  - [6] A. A. Houck, J. B. Brock, I. L. Chuang, *Phys. Rev. Lett.* **90**, 137401 (2003).
  - [7] N. Fang, H. Lee, C. Sun, and X. Zhang, *Science* **308**, 534 (2005).
  - [8] Z. M. Zhang and C. J. Fu, *Appl. Phys. Lett.* **80**, 1097 (2002).
  - [9] K. Y. Kim, *Phys. Rev. E* **70**, 047603 (2004).
  - [10] J. A. Kong, B. Wu, and Y. Zhang, *Appl. Phys. Lett.* **80**, 2084 (2002).
  - [11] P. R. Berman, *Phys. Rev. E* **66**, 067603 (2002).
  - [12] D. Rozas, C. T. Law, and G. A. Swartzlander Jr., *J. Opt. Soc. Am. B* **14**, 3054 (1997).
  - [13] D. G. Grier, *Nature (London)* **424**, 810 (2003).
  - [14] J. E. Curtis and D. G. Grier, *Phys. Rev. Lett.* **90**, 133901 (2003).
  - [15] I. V. Basistiy, M. S. Soskin, and M. V. Vasnetsov, *Opt. Commun.* **119**, 604 (1995).
  - [16] L. Allen, M. W. Beijersbergen, R. J. C. Spreeuw, and J. P. Woerdman, *Phys. Rev. A* **45**, 8185 (1992).
  - [17] M. J. Padgett and L. Allen, *Opt. Commun.* **121**, 36 (1995).
  - [18] L. Allen and M. J. Padgett, *Opt. Commun.* **184**, 67 (2000).
  - [19] A. E. Siegman, *Lasers* (University Science, Mill Valley, 1986).
  - [20] H. Luo, Z. Ren, W. Shu, and F. Li, *Phys. Rev. E* **75**, 026601 (2007).
  - [21] J. W. Goodman, *Introduction to Fourier Optics* (McGraw-Hill, New York, 1996).
  - [22] I. S. Gradshteyn and I. M. Ryzhik, *Tables of Integrals, Series, and Products* (Academic, San Diego, CA, 1980).
  - [23] M. Lax, W. H. Louisell and W. McKnight, *Phys. Rev. A* **11**, 1365 (1975).
  - [24] P. Hariharan and P. A. Robinson, *J. Mod. Opt.* **43**, 219 (1996).
  - [25] S. Feng, H. G. Winful, *Opt. Lett.* **26**, 485 (2001).
  - [26] A. V. Volyar, V. G. Shvedov, and T. A. Fadeeva, *Tech. Phys. Lett.* **25**, 203 (1999).
  - [27] R. Loudon, *Phys. Rev. A* **68**, 013806 (2003).
  - [28] M. J. Padgett, S. M. Barnett and R. Loudon, *J. Mod. Opt.* **50**, 1555 (2003).
  - [29] J. A. Kong, *Electromagnetic Wave Theory* (EMW Publishing, Cambridge, MA, 2005).
  - [30] B. A. Kemp, T. M. Grzegorzczak and J. A. Kong, *Opt. Express* **13**, 9280 (2005).
  - [31] J. D. Jackson, *Classical Electrodynamics* (Wiley, New York, 1999).
  - [32] L. D. Landau, E. M. Lifshitz, and L. P. Pitaevskii, *Electrodynamics of Continuous Media* (Pergamon, New York, 1984).
  - [33] B. A. Kemp, J. A. Kong and T. M. Grzegorzczak, *Phys. Rev. A* **75**, 053810 (2007).
  - [34] J. Courtial and M. J. Padgett, *Opt. Commun.* **173**, 269 (2000).
  - [35] J. Leach, S. Keen, M. J. Padgett, C. Saunter, G. D. Love, *Opt. Express* **14**, 11919 (2006).
  - [36] M. J. Padgett, J. Alrt, N. Simpson and L. Allen, *Am. J. Phys.* **64**, 77 (1996).
  - [37] M. S. Soskin, V. N. Gorshkov, M. V. Vasnetsov, J. T. Mallos and N. R. Heckenberg *Phys. Rev. A* **56**, 4064 (1997).
  - [38] M. P. MacDonald, K. Volke-Sepulveda, L. Paterson, J. Arlt, W. Sibbett, and K. Dholakia, *Opt. Commun.* **201**, 21 (2002).